The hemolymph of *Biomphalaria* snail vectors of schistosomiasis supports a diverse microbiome

Frédéric D. Chevalier*, Robbie Diaz, Marina McDew-White, Timothy JC. Anderson, Winka Le Clec'h*

Texas Biomedical Research Institute, PO Box 760549, San Antonio, TX 78258

Author information:

- Frédéric D. Chevalier* : fcheval@txbiomed.org - ORCID: 0000-0003-2611-8106
- Robbie Diaz : robbied@txbiomed.org
- Marina McDew-White: mwhite@txbiomed.org - ORCID: 0000-0001-7821-260X
- Timothy JC. Anderson: tanderso@txbiomed.org - ORCID: 0000-0002-0191-0204
- Winka Le Clec'h*: winkal@txbiomed.org – ORCID: 0000-0002-1111-2492

* Corresponding authors

Running title: The hemolymph microbiome of Biomphalaria snails

ABSTRACT

The microbiome – the microorganism community that is found on or within an organism's body – is increasingly recognized to shape many aspects of its host biology and is a key determinant of health and disease. Microbiomes modulate the capacity of insect disease vectors (mosquitos, tsetse flies, sandflies) to transmit parasites and disease. We investigate the diversity and abundance of microorganisms within the hemolymph (*i.e.* blood) of *Biomphalaria* snails, the intermediate host for *Schistosoma mansoni*, using Illumina MiSeq sequencing of the bacterial 16S V4 rDNA. We sampled hemolymph from 5 snails from 6 different laboratory populations of *B. glabrata* and one population of *B. alexandrina*. We observed 281.34 ± 0.81 amplicon sequence variants (ASVs) per snail. There were significant differences in microbiome composition at the level of individual snails, snail populations and species. Snail microbiomes were dominated by Proteobacteria and Bacteroidetes while water microbiomes from snail tank were dominated by Actinobacteria. We investigated the absolute bacterial load using qPCR: hemolymph samples contained 2,620 ± 321 bacteria per µL. We speculate that the microbiome may represent a critical, but unexplored intermediary in the snail-schistosome interaction as hemolymph is in very close contact to the parasite at each step of its development.

INTRODUCTION

The microbiome – the community of microorganisms that inhabit both the human body and that of multiple other phyla [1] – is increasingly recognized to play a critical role in many aspects of biology and as a key determinant of health and disease. For example, the human gut microbiome is thought to play a role in the development of diabetes, rheumatoid arthritis, muscular dystrophy, multiple sclerosis, and obesity [2]. In invertebrates, symbiotic bacteria are involved in synthesizing essential amino acids or vitamins [3, 4], in digesting cellulose [5], in protection against parasites [3], in feminization and parthenogenesis [6], and even in speciation [7].

In host-parasite interactions, the host microbiome frequently plays an important role in the ability of parasite to colonize its host. This tripartite interaction (i.e. host-microbiome-parasite/pathogen) has been investigated widely in invertebrate hosts. Recent research on the widespread endosymbiotic bacteria *Wolbachia* demonstrates that *Wolbachia*-infected mosquitoes are unable to transmit dengue fever [8]. This bacterium is now a major focus of efforts to control or eliminate dengue, and has stimulated new interest in utilizing bacterial symbionts to modify disease vectors [8]. Similarly, the aphid microbiome protects these insects against parasitoid wasps [3], the microbiome of sandflies provides protection against *Leishmania* infection [9], while the microbiome of mosquitoes and tsetse flies impedes infection by malaria parasites and trypanosomes respectively [10].

Among human helminth parasites, schistosomes are the most important, infecting over 206 million people in 78 countries in 2016 [11], and causing more than 200,000 deaths per year. Schistosome parasites have a complex lifecycle, involving a freshwater snail as intermediate host and a mammal as a definitive host. In humans, adult trematodes live in the blood vessels surrounding the intestine, and pathology results from immune reactions to eggs which become trapped in the liver, resulting in granulomas, calcification of blood vessels, portal hypertension and liver failure [12, 13]. There is no licensed vaccine, and control is reliant on a single monotherapy (praziquantel) to which resistance has been recorded, so there is an urgent need for

alternative approaches to parasite control. Understanding the snail-schistosome interaction is therefore critical to develop these kind of approaches. When a single parasite larva (miracidium) penetrates a snail, this develops into a primary sporocyst, which then divides asexually to generate multiple clonally-produced secondary sporocysts in the snail tissue. These produce hundreds to tens of thousands of motile cercariae larvae that are released into the water where they penetrate and infect the definitive host (human or rodent). Snail populations vary in susceptibility to schistosomes [14] and while genetics certainly plays a role [15], the mechanisms determining whether infections develop are poorly understood and the influence of the microbiome on schistosome parasite development is currently unknown.

The *Biomphalaria* snail microbiome was firstly characterized using classical microbial culture methods and biochemical characterization almost 40 years ago [16]. Bacteria were found in the whole snail but also on its surface, gut and body cavity. With this relatively limited technique, the authors observed changes in whole snail microbiome when those were moved between different environments [16]. More recently, two papers [17, 18] have examined *Biomphalaria* spp. microbiomes using deep sequencing of rDNA. Allan *et al.* [17] showed that snails carrying alleles conferring resistance to *S. mansoni* infection, show distinctive microbiomes from those carrying sensitive alleles, suggesting possible links between the microbiome composition and *S. mansoni* susceptibility. Huot *et al.* [18] examined core microbiomes from several laboratory populations, showing a high specificity between these microbiomes and their snail host populations, as well as complete congruence between core microbiome and host phylogeny. Importantly, both these studies examined microbiomes of whole snails, so it is unclear whether the bacteria characterized are from the gut, shell surface, mantle cavity or internal organs of the snail, each of which may have a distinctive microbiome. Rather than characterize composite microbiomes from whole snails, we focus on the microbiomes from a single tissue – the hemolymph (*i.e.*, invertebrate blood). We chose this tissue, because, developing schistosome parasites are in continuous contact with the snail hemolymph during the 30-day development until the first parasite larvae emerge from the mollusk, so the hemolymph microbiome is likely to be most relevant for understanding interactions between

snails, bacteria and developing schistosomes. Furthermore, evidence from other mollusk species provide a precedent for investigating the *Biomphalaria* microbiome: hemolymphs from several fresh or seawater mollusks are known to harbor specific microbiomes [19, 20] that can be modified by environmental stress [21], pollutants [22] or pathogens [21, 23].

In this study, we characterized the hemolymph microbiome of two *Biomphalaria spp.* freshwater snail species (i.e. *B. glabrata* and *B. alexandrina*), both vectors of *Schistosoma mansoni* using a 16S rDNA approach. We demonstrate that snail hemolymph harbors a diverse microbiome, and that that different *Biomphalaria* species and populations harbor distinctive hemolymph microbiomes that are independent of the water environment. As the microbiome is critical in other host-parasite systems we speculate that it may represent a critical, but unexplored, intermediary in the snail-schistosome interaction.

MATERIALS AND METHODS

1) Biomphalaria spp. *hemolymph collection*

Biomphalaria spp. freshwater snails are intermediate host for schistosome trematode parasites. In this study, we sampled only hemolymph (i.e. blood) from uninfected snails. All our *Biomphalaria spp.* snails are reared in 10-gallon aquaria containing aerated freshwater at 26-28°C on a 12L-12D photocycle and fed *ad libitum* on green leaf lettuce. An advantage of *Biomphalaria* snails is their large size and their flat shell. This allow easy access to the heart and makes collection of ~80-100 µL of hemolymph possible. All snails used in this study had a shell diameter between 10-15 mm. For each individual snail, we disinfected the shell with 70% ethanol, and collected the hemolymph by heart puncture using a sterile 1 mL syringe and a sterile 22 gauge needle. The hemolymph collected was immediately placed in a sterile 1.5 mL pre-cooled microtube on ice. We collected hemolymph from 5 individual snails from each of 7 different populations of *Biomphalaria spp.* (Table 1, Figure 1). We also sampled water from the aquaria where each *Biomphalaria spp.* populations were raised as a control, to characterize the microbiome from the snails' environment. Immediately after collection, samples were snap-frozen in liquid nitrogen and stored at -80˚C until processing.

2) 16S rDNA library preparation and sequencing

We extracted DNA from the snail hemolymph and water samples using the Blood and Tissue kit (Qiagen), following the manufacturer protocol, with minor modifications. To verify the reproducibility of our process for DNA extraction, library preparation and sequencing, we split each hemolymph or water sample in two aliquots and processed them independently. For each replicate sample, we extracted total DNA using 40 µL of the hemolymph or water samples. We incubated each replicate 45 minutes at 56˚C in a water bath. We recovered final gDNA in 50 µL of elution buffer (Qiagen).

We prepared the 16S rDNA libraries under a biosafety cabinet to avoid contamination, and in triplicate to avoid biases potentially introduced during PCR reaction step. We amplified 250 bp of the 16S rDNA V4 region from bacteria and archaea, using specific primers (515f and 806rB) designed by the Earth Microbiome Project [24]. Each 515f forward primers were barcoded to allow the identification of samples. The 16S rDNA V4 reaction mixture consisted of 4 µL of 1X 5 Prime Hot Master Mix (QuantaBio), 2 µL of sterile water, 1 µL of 2 µM 515f barcoded primer, 1 µL of 2 µM 806rB primer (Supp. Table 1), and 2 µL of total gDNA template. Libraries are amplified using the GeneAmp PCR system 9700 (Applied Biosystems) as follows: 95°C for 3 minutes, then 35 cycles of 95°C for 45 seconds, 50°C for 1 minute, 72°C for 90 seconds, then 72°C for 10 minutes. We electrophoresed 2 µL of each PCR product on agarose gel (2%) to check amplicon size, and absence of contamination in the controls. We pooled the triplicate PCR products for a final volume of 24 µL and purified the PCR product by adding 44 µL of AMPure XP beads (Beckman Coulter), mixing with pipette and, incubating the samples (5 minutes). We separated the beads on a 96 well-plate magnetic device (5 minutes), discarded the cleared solution from each well, and washed beads twice in 200 µL of freshly-prepared 70% ethanol (1 minute), while maintaining the plate on the magnetic device. After drying beads (3 minutes), we incubated each sample in 20 µL of nuclease-free sterile water after mixing by pipetting (2 minute), separated the beads on the magnetic device (3 minutes) and placed the purified 16S rDNA V4 barcoded libraries in a fresh 96 well-plate. All incubations were done at room temperature. We quantified these libraries using Picogreen quantification assay (Invitrogen) following the manufacturer's instructions. Finally, we made an equimass pool of all the libraries using 15 ng of each library. We quantified the final pool fragment size using the 4200 TapeStation (DNA screen tape, Agilent Technology) and molarity using the Kappa library quantification kit for the Illumina sequencing platform (following the manufacturer's recommendations). We sequenced the pool on an Illumina MiSeq sequencer at Texas Biomedical Research Institute (San Antonio, Texas). Raw sequencing data are accessible from the NCBI Sequence Read Archive under BioProject accession number PRJNA613098.

3) Sequence processing

Commands and scripts used for the sequence processing and downstream analysis are available in a Jupyter notebook on Github.

We demultiplexed the raw sequencing data obtained from the MiSeq using bcl2fastq (v2.17.1.14, Illumina) with the default parameters. We used the fastq files generated as input for Qiime2 (v2019.4) [25]. We checked the read quality from the results of the demux module. We then denoised and clustered the sequences into amplicon sequence variants (ASVs) using the denoise-paired command from the dada2 module with a max expected error of 5. We determined the taxonomy of the ASV using the classify-consensus-vsearch command of the feature-classifier module using a 97% identity threshold. To build a phylogenetic tree, we aligned the ASVs and masked the highly variable positions using the mafft and mask commands from the alignment module. Finally, we built and rooted a tree from the alignment using the fasttree and midpoint-root commands from the phylogeny module.

4) Functional inference of the microbiome

We inferred the microbiome's function using PiCRUST2 software (v2.1.4b). We used the Qiiime2 processed data and exported the ASV representative sequences of the taxonomy analysis and the abundance table. We placed the sequences into the reference tree, performed hidden-state prediction of gene families and generated metagenome prediction. We performed pathway-level inference and finally add functional description to the generated files. Finally, we performed a differential pathway abundance using the ALDEx2 R package (v1.16.0) [26] on the unstratified pathway prediction.

5) Estimation of bacterial abundance by quantitative PCR

We performed real time quantitative PCR (qPCR) reactions to estimate the number of bacterial 16S rDNA in each hemolymph and water replicated sample. Reactions were performed in duplicate using the QuantStudio 5 (Applied Biosystems) as follows: 95°C for 10 minutes, then 40 cycles of 95°C for 15 seconds and 60°C for 1 minute. Duplicate reactions showing a difference in C_T greater than one were rerun. The reaction mixture consisted of 5 µL of SYBR Green MasterMix (Applied Biosystems), 0.3 µL of 10 µM forward primer (515f without barcode: GTGYCAGCMGCCGCGGTAA) and 10 µM reverse primer (806rB: GGACTACNVGGGTWTCTAAT) amplifying 250 bp of the 16S rDNA V4 region, 3.4 µL of sterile water and 1 µL of total DNA template. We plotted standard curves using seven dilutions of a purified 16S V4 rDNA amplicon (copies.μL^{-1}: 1.34×10^1, 1.34×10^2, 1.34×10^3, 1.34×10^4, 1.34×10^5, 1.34×10^6, 1.34×10^7). We produced the purified 16S V4 rDNA by amplification of the V4 region of *Escherichia coli* XL 10-gold (Agilent) using TaKaRa Taq R001 AM kit (Clonetech) following the manufacturer's protocol (PCR cycles: 95˚C for 10 min, [95˚C for 15 s, 50˚C for 30 s, 60˚C for 60 s] × 35 cycles, 60˚C for 10 min). We purified the PCR product using AMPure XP beads (Beckman Coulter) following the manufacturer's protocol, and quantified it using Qubit dsDNA BR Assay kit (Invitrogen). We determined the number of copies in the PCR product as follows: PCR product length × (average molecular mass of nucleotides (330 $g.mol^{-1}$) × 2 strands) × Avogadro constant. The number of 16S V4 rDNA V4 copies in each sample was estimated according to the standard curve (QuantStudio Design and Analysis Software). The primer pair (515f/806rB) was chosen to allow direct comparison of qPCR values with Illumina MiSeq sequenced amplicons of the same locus. We corrected the 16S copy number from the qPCR using the dilution factor between hemolymph and elution volume (40 and 50 µL, respectively). We normalized the values using the estimated 16S copy per bacteria from PiCRUST2 and the abundance of each bacteria from Qiime2 (see section 5).

6) Statistical analysis

All statistical analyzes and graphs were performed using R software (v3.5.1). We used several packages to compute diversity statistics from the Qiime data: phyloseq (v1.26.1) [27], microbiome (v1.8.0), and picante (v1.8.1) [28]. We compared α-diversity results using a pairwise Wilcoxon test. We used the vegan (v2.5.4) and the pairwiseAdonis (v0.0.1) packages to perform β-dispersion and Permanova tests, respectively.

We compared the microbial density between populations using Kruskal-Wallis test (data not following normal distribution; Shapiro test, $p < 0.05$) followed by pairwise comparison post-hoc test. We used Kendall's tau coefficient to test the correlation between the estimated bacteria density and the observed microbial richness. The confidence interval of significance was set to 95% and *p*-values less than 0.05 were considered as significant.

RESULTS

1) Library statistics

We sequenced snail hemolymph and water samples from seven populations (Table 1). For each population, we collected hemolymph from five snails and a sample of the tank water they were collected from. To test the reproducibility of our protocol, we split each sample and prepared libraries independently for each half (Fig. 1). After MiSeq sequencing, we obtained an average of 155,491.5 ± 29,277.9 reads per library (mean ± s.d.) (Supp. Table 2). We retained on average 87 ± 0.04% of the initial reads after sequencing error filtering, 85 ± 0.03% of the initial reads after denoising the data using the dada2 module, 73 ± 0.05% of the initial reads after merging reads and 71 ± 0.06% of the initial reads after removing chimeras. Sequencing depth was relatively even between sample types and replicates (Supp. Table 2). Rarefaction curve analysis of each library showed a plateau, indicating that our sequencing effectively captured the microbiome diversity (Fig. 2). Taxonomy assignment of the 16S rDNA sequences from all libraries revealed a total of 2,688 amplicon sequence variants (ASVs).

2) Microbiome diversity

a) α diversity (microbial diversity within samples)

We computed several α diversity indices (Table 2) to investigate the bacterial richness (the number of taxa) and diversity (a composite measure of richness and abundance of bacterial taxa) within hemolymph and water samples (Fig. 3). The observed species richness and the Chao1 index revealed that snail hemolymph had higher bacterial richness than water, with the exception of the BgNMRI population. Overall, we found twice the number of ASV in snail hemolymph (281.34 ± 0.81; mean ± s.e.) than in the tank water (145.57 ± 4.04). Most of the snail populations showed similar richness, with Bg26 showing the highest and BgNMRI the lowest. The close

similarity between the observed richness and the Chao1 index plots suggests that we effectively captured rare taxa, consistent with the rarefaction analysis.

The bacterial richness of the hemolymph is correlated with a higher bacterial diversity as expected. The Shannon diversity index showed lower diversity in the water when compared to the hemolymph. Among the snail populations, we observed the highest diversity in Bg26 and Bg121 and the lowest in Bg36 and BgNMRI. Individuals from the BgBS90 population showed the greatest variability between snails suggesting high heterogeneity in this population. The Faith's phylogenetic diversity showed a similar trend: we observed a lower diversity in the water while hemolymph displayed similar diversity across snail populations. This suggests that the differences observed between the Shannon index and the phylogenetic diversity is likely due to presence of rare taxa.

The Simpson indices for evenness and dominance were low for both hemolymph and water samples, in accordance with the over representation of particular taxa. Hemolymph from Bg36 population, closely followed by Ba and BgB90 populations, showed the lowest evenness and the highest dominance of the snail populations. BgNMRI snails, which had similar richness and diversity profile as Bg36 snails, showed slightly more evenness in their bacterial community and an intermediate dominance. Water samples, which consistently showed low richness and diversity, had a comparable evenness to snail samples but stronger dominance consistent with the Shannon diversity index.

Data from the replicated libraries showed similar results. We obtained a strong correlation ($0.85 < R^2 < 0.98$, $p < 0.01$) between the replicated libraries (Supp. Fig. 1) when comparing the different indices, highlighting the robustness and reproducibility of our protocol.

b) β diversity (microbial diversity between samples)

We computed several β diversity indices to investigate how the bacterial communities discriminate each snail population (Fig. 4). We first compared microbiomes using qualitative metrics that are based on the presence or absence of bacterial taxa (Jaccard index) adjusted with phylogenetic distance (unweighted unifrac index), independently of taxa abundance. We statistically compare these metrics using Permanova analysis. These analyses demonstrate that water samples have significantly different bacterial communities from the snail populations. Similarly, all pairwise comparisons between snail communities showed statistically different composition. In addition, the Jaccard index and, to a lesser extent, the unweighted unifrac reveal clear groups: (i) Ba is distant from all Bg snail populations strongly suggesting that hemolymph microbiome can discriminate snail species; (ii) Two clusters of Bg snails can be identified: the first cluster comprises BgBS90, BgBRE, Bg121 and Bg36 (all from Brazil) and the second cluster comprises Bg26 and BgNMRI (from Carribbean).

We also compared populations of snails or water microbiome for the Jaccard and unweighted unifrac indices using a β dispersion test (Fig. 4A-B). This test compares the homogeneity of β-diversity measures across different sampling units (individual snails, or water from different tanks) between populations. All the snail populations showed similar variance when compared to each other. In contrast, the water population showed over dispersion when compared to all the snail populations. This may be explained by the fact that samples of water come from different aquariums, each of them carrying characteristic bacteria, while individual snails within a population come from the same tank.

We performed similar comparisons using quantitative metrics that take into account the abundance of each bacterial taxa (Bray index) adjusted with phylogenetic information (weighted unifrac index). Comparisons of Bray indices using a permanova analysis revealed that all snail populations and water showed different composition from each other (Fig. 4C). We obtained similar results when adding phylogenetic information (Fig. 4D) except for the pairs Bg121-Bg36 and BgBS90-BgNMRI, suggesting that these microbiomes shared similar abundant taxa between these pairs (Fig. 4D). These results suggest that abundant bacterial taxa drive the

distinction between populations and revealed similar microbiomes in some genetically related snail populations (Bg121-Bg36).

c) Taxonomic diversity

We found dramatic differences between populations in terms of taxonomic composition of bacteria (Fig. 4). Hemolymph microbiomes were dominated by bacteria from the phyla Proteobacteria (in all Bg populations) and Bacteroidetes (in Ba population) while water microbiomes were dominated by bacteria from the Actinobacteria phylum. These differences in dominating phyla reflect the previous observations from the β diversity analyses: a clear distinction (i) between the water and snails and (ii) between the two snail species (i.e., Bg and Ba). We also observed differences in proportion of bacteria from minor phyla among the different snail populations. For instance, Bg26 showed a greater proportion of Acidobacteria while BgNMRI and Ba showed the lowest proportion of Verrucomicrobia. These differences may reflect differences in the physiology of these different populations. Microbiomes from snail samples (and at a lesser extent from water samples) contained also a relatively high proportion of bacteria with unassigned taxa: 5% to 43% of bacteria from snails while 0.2% to 18% of bacteria from the water were uncharacterized.

Individual snails from a population tended to show a similar taxonomic composition as they clustered together (Fig. 5A). The relatedness between populations reflects what is observed with the qualitative analysis of the β diversity (Fig. 4C-D). When comparing individuals within a population (Fig. 5B), we observed variation in the relative taxa abundance. For instance, individuals from the Bg26 showed a more homogeneous composition than Ba snails which tended to show the highest variability.

The analysis of the 50 most abundant ASVs present in each populations revealed that a high proportion of these ASVs are specific to a population while some of these ASVs are shared across all the snail populations (Supp. Fig. 2). We observed variation between individual snails of the same population: some ASVs were

abundant in some snails, but absent from other individuals. The most abundant ASVs in snail samples were not abundant in water sample, confirming the results observed with the global composition (Fig. 4)

The reproducibility of our protocol is again confirmed in this analysis (Supp. Fig. 3). All the replicated libraries clustered together with the exception of one BgNMRI sample.

3) Microbiome density

We investigated the bacterial density by performing real time quantitative PCR on our samples, and corrected the results to estimate the number of bacteria (Fig. 6A-B). We quantified an average of 4,490 16S rDNA copies per µL of sample (range: 186 to 59,487). We found the highest average copy number in BgNMRI and the lowest in BgBRE and water (Fig. 6A) (Kruskal-Wallis test: X^2=26.494, df=7, p=0.0004108 followed by post-hoc pairwise comparison test).

Bacteria usually carry more than one 16S gene copy in their genome [29]. We corrected the raw density data based on 16S copy number using the estimation of 16S copy number per ASV computed by PiCRUST2. This normalization gave an average of 2,620 ± 321 (mean ± s.e.) (range: 172 to 16,453) estimated bacteria per µL in snail samples and 1,330 ± 373 in water samples (range: 166 to 4,944) (Fig. 6B). This did not change drastically the trend already observed with the raw copy number quantification. We narrowed the global and per population variation and observed significant differences only between BgNMRI and BgBRE (Kruskal-Wallis test: X^2=18.294, df=7, p=0.01071 followed by post-hoc pairwise comparison test). When considering an average volume of 100 µL of hemolymph per adult snail (personal observation) and an average of 2,620 estimated bacteria per µL in snail individuals, the snail hemolymph should be inhabited by an average of 260,000 bacteria (range: 17,200 to 1,645,300).

We examined the correlation between the estimated bacteria density and the observed microbial richness diversity. We found no correlation (Kendall's τ=-0.076, p-value=0.3). This confirms that we can safely estimate microbial diversity without taking in account bacterial density.

4) Functional inference of the hemolymph microbiome

The microbiome in hemolymph could have a functional role in the snail physiology, just as the gut microbiome does in humans [30]. We investigated the presence of particular metabolic pathways in snails and water samples based on 16S taxonomy using the PiCRUST2 pipeline. We identified 15 and 4 pathways overrepresented in hemolymph and water samples, and supported by our two technical replicates (Supp. tab. 3). The 15 overrepresented pathways in hemolymph were involved in synthesis of vitamins/electron transporters and amines, degradation of sugar and amines, and fermentation.

The pathway overrepresented in water samples were involved in synthesis of molecules related to cell wall, DNA synthesis, and detoxification. At least two out of the four overrepresented pathways are found in bacteria from the Actinobacteria phylum, the dominant phylum found in water.

In both snail and water samples, other differentially represented pathways were found in only one of the two technical replicates. This could be due to differences in taxa representation and abundance and highlight the sensitivity of metabolic inference to this factor.

DISCUSSION

1. Snail hemolymph supports a diverse microbiome.

We have unambiguously showed the presence of diverse microbiomes in the snail hemolymph of one population of *Biomphalaria alexandrina* and six populations of *B. glabrata.* The snail microbiome contains hemocytes that protect against incoming microbes, so the existence of a flourishing microbiome in the hemolymph might seem surprising to some. Two lines of argument suggest that the hemolymph microbiomes we have described are real, rather than an artifact of our collection procedure (for example, resulting from trace contamination with the water microbiome inside the mantle, during syringe penetration).

(i) The bacterial diversity of the snail microbiomes is distinctive from that of the water in the tanks. The hemolymph and water microbiome showed dramatic differences in dominating phyla (Proteobacteria (for all the Bg populations), Bacteroidetes (for the Ba population), and Actinobacteria phylum in the water microbiomes). The hemolymph microbiomes were more diverse than the water microbiomes using multiple different diversity metrics. Finally, different species or populations of snails show characteristic bacterial composition in their hemolymph. The hemolymph, and to a lesser extent, the water samples harbor uncharacterized taxa: a third of the ASVs identified did not have a taxonomic assignment.

(ii) Bacteria were abundant in the hemolymph. We observed an average of 2,620 bacteria per microliter of snail hemolymph, with a maximum of 16,453 in the BgNMRI population. Assuming 100µL hemolymph per snail this equates to 262,000 bacteria, or 1,645,300 for BgNMRI.

Our demonstration that the *Biomphalaria* hemolymph contains a rich microbiome is consistent with published reports detailing the microbiome from other mollusks, crustaceans [19, 20, 31, 32] and also from insects [33].

The intimate relationship between these organisms and their water environment and their semi-open vascular system may prevent them from having a sterile hemolymph. Instead, they may use a tolerance strategy as observed in the human gut [34]. In insects, the presence of both transient and obligate bacteria in the hemolymph is now recognized [33] but only few bacterial taxa can survive in such environment. In contrast, our results show that the hemolymph of *Biomphalaria* snails is inhabited by a highly diverse microbiome, suggesting that the snail hemolymph environment is more permissive.

2. Does genetics or environment drive microbiome differences?

Differences in microbial diversity between hemolymph samples reflected their species or populations of origin. At the species level, *B. glabrata* and *B. alexandrina* always clustered apart based on both qualitative and quantitative β diversity analysis. This was driven by the differences in bacterial taxa and their abundance between the two species despite the fact that all these snails were exposed to the same water and food. Therefore, the differences in the microbial composition are likely to be genetically controlled, reflecting the evolutionary distance between the two species. At the population level, we could discriminate *B. glabrata* populations based on rare taxa (qualitative β diversity analysis). Interestingly, the distance between population clusters was consistent with geographical origins: Brazilian populations (BgBRE, BgBS90) clustered apart from the Caribbean population (BgNMRI), while inbred subpopulations from a cross between snails of Caribbean and Brazilian origin [35] tended to cluster with the Caribbean population (Bg26) or the Brazilian population (Bg36, Bg121). If genetics is the main driver, this would suggest that the mechanism of microbiome selection at the population level is different from the mechanism acting at the species level. However, a strong influence of the environment could also explain this result: we sampled snails of each population from single tanks. The rare taxa distinguishing microbiomes from different snail populations could also be a signature of the tank microbiome.

An association between snail genetics and the composition of whole snail microbiome has been observed previously [17]. In this particular case, specific genotypes at a locus involved in snail compatibility with schistosome infection were linked to changes in two particular taxa (*Gemmatimonas aurantiaca* and *Micavibrio aeruginosavorus*). This locus likely contains immune genes that could specifically shape the whole snail microbiome. In addition, a recent analysis of whole snail microbiomes that included several *Biomphalaria* species and *B. glabrata* populations is consistent with our observation regarding species differentiation based on microbiome but failed to support *B. glabrata* population differentiation [18]. Three factors from the Huot *et al.* [18] study could explain this difference: (i) the shell was removed prior to DNA extraction: this may have resulted in significant loss of hemolymph, reducing the contribution of hemolymph to the results, or (ii) their analysis focused on the core microbiome: excluding rare taxa may have limited their ability to detect population differentiation, or (iii) the composite microbiome from whole snails (including microbiomes from multiple different organs) was analyzed.

Past studies on whole snail microbiomes using older, culture-based methodology showed a strong influence of the environment: translocating *B. glabrata* from one river to another had a dramatic impact on abundance of cultivable bacteria [36]. This change in microbiome could be due to uptake of new bacteria from this new environment or could result from the stress of the translocation leading to the modification of the immune system and consequently of the microbiome composition. To better understand the relative role of genes and environment in controlling microbiome composition, classical genetic crosses, and common garden rearing experiments will be needed.

3. Origin of the hemolymph microbiome

Microorganisms can be acquired directly from the environment or transmitted vertically from the parents. We observed shared bacterial taxa between snail hemolymph and water suggesting that exchanges between the

environment and the snail is likely to occur. Exchange could takes place at two main sites: the mantle cavity and the gut. The mantle cavity is likely involved in gas exchange between the hemolymph and the water [37]. The structure of this cavity is designed to maintain a continuous water flow with an extensive surface of exchange. Loose vascular connective tissue has been observed under the ciliated epithelium [38]. This cavity seems able to absorb particles through pinocytosis suggesting that active uptake occurs at the epithelium [38]. In addition, snails easily release hemolymph after deep retraction in its shell [39] suggesting a relative fragility of this epithelium. Therefore, the mantle epithelium could be a portal for active or passive acquisition of microorganisms. The gut could be another site where such acquisition can take place. The midgut gland (i.e., hepatopancreas) actively phagocytizes particles [40]. A complex microbiome exists in the snail gut [41] and bacteria could be phagocytized by the hepatopancreas cells and reach the hemolymph either after active selection or before being fully degraded by the snail cells. There is evidence that gut and hepatopancreas can be infected by amoebae [42] and microsporidia [43]. One particular microsporidium, *Capsaspora owczarzaki*, was found in the mantle and pericardial explants strongly suggesting that microorganisms can pass the mantel cavity [44, 45]. It is likely that other microorganisms could use the same paths to reach the hemolymph.

A second route of microbiome acquisition is a vertical transmission from parents to offspring. Microorganisms could be selectively added to the egg yolk or the egg mass fluid (i.e. fluid surrounding the eggs inside the egg mass) and could be integrated into the developing organism. Antimicrobial proteins have been identified in both egg yolk [46] and egg mass fluid [47] which, in addition of protecting the eggs from outside pathogens, could control the development of the transmitted microbiome. Vertical transmission of microorganisms via the egg cytoplasm [6] or after spreading them on the egg surface [48, 49] is common in invertebrates but is limited to a few bacterial species. However vertical transmission of complex microbiome can occur: recent studies have demonstrated the presence of a microbiome in amniotic fluid in humans [50]. It is possible that vertical transmission of complex microbiomes is more common than currently thought.

4. *Microbiome functionality: clandestine passenger or good citizen*

The primary role of the hemolymph is to distribute nutrients to organs and defend the snail against infections. The presence of a microbiome could result from a tolerance strategy to mitigate the high costs of a maintaining a sterile hemolymph and could be comprised of commensal microorganisms only. However, snails could have evolved in order to take advantage of the presence of this microbiome. Hemolymph microbiomes could be involved in providing nutrients to its snail host. Pathway inference analysis from our microbiome data showed that hemolymph microbiome is enriched in pathways related to vitamin production. Vitamins are known to be essential in egg production: snails raised in axenic condition were not able to lay eggs except with a supplement of vitamin E [51]. We did not find pathways involved in the production of this particular vitamin but for others (B6, B12, K12) which may also have a role in snail physiology. The vitamins B6 (pyridoxine), B12 (cobalamin), and K12 (menaquinol) are essential to animals and could be released into the hemolymph by the bacteria and absorbed by the snail tissues. We have also shown enrichment for other pathways like sugars and polyamines which could serve only bacteria but could also be beneficial to snail hosts. Sugar degradation is likely involved in energy generation for the bacteria. Polyamines are linked to bacterial growth and survival by reducing oxidative stress [52] which could be generated by the presence of the hemocytes [53]. Production of critical metabolites by the hemolymph microbiome could support sustainable production of these metabolites.

This microbiome could also be involved in snail defense either directly by controlling pathogens or indirectly by stimulating the snail immune system or competing with pathogens. Snails are susceptible to pathogens ranging from bacteria [54] to multicellular parasites [55] such as schistosomes causing damages to the snail organs.

5. *Role of the hemolymph microbiome in the snail-schistosome interactions*

We hypothesize that hemolymph microbiome could be a third player in the interaction between the snail and its schistosome parasite. The hemolymph is known to be involved in snail defense against schistosomes by the action of hemocytes and humoral factors [53]. Snail genetics has also been shown to be a major determinant of snail resistance [15]. However, the microbiome could enhance or reduce snail resistance. Enhancing resistance could occur by direct interaction with the parasite (through competition or parasite infection) or by stimulation of the immune system. The microsporidia *C. owczarzaki* showed direct interaction with *S. mansoni* sporocysts leading to their death while leaving the snail unharmed [44, 45]. These microsporidia were found in higher density in resistant snail populations [44]. This could result from resistant snail actively selecting this particular microorganism. Furthermore, the abundance of particular bacterial taxa in whole snails has been associated with snail genotypes linked to schistosome resistance [17]. While it is unknown if the bacteria associated with the resistant genotype are actually involved in resistance, this showed that genetic control of microbial composition occurs in snails and could influence interactions between snails and schistosomes.

In addition to the fact that *Biomphalaria spp*. snails are intermediate hosts of *S. mansoni*, these snails have several attractive features that make them a promising model system for studying invertebrate-microbiome interactions. Namely (i) they are easy to grow in large numbers in aquaria or plastic trays and experimentally tractable, (ii) they are relatively large and hemolymph can be easily sampled (iii) as these snails are hermaphrodite, inbred snail lines are easily generated by serial inbreeding to minimize host genetic effects [35], (iv) improving genomic resources and tools for gene silencing are available [56, 57]. We anticipate that *Biomphalaria spp*. may join the list of non-traditional model invertebrate species [58] that are now being exploited for asking both pure and applied questions about microbiome biology.

ACKNOWLEDGMENTS

We thank Michael S. Blouin from Oregon State University for providing all the inbred *Biomphalaria glabrata* snail lines (Bg26, Bg36 and Bg121) , Guillaume Mitta and Benjamin Gourbal (University of Perpignan, France) for providing the BgBRE snails, Philip LoVerde (UT Health, San Antonio) and the Biomedical Research Institute (NIAID Schistosomiasis Resource Center, Rockville, MD) for providing the BgNMRI and BgBS90 snails through NIH-NIAID Contract HHSN272201700014I, and the Theodor Bilharz Research Institute (Giza, Egypt) for providing *B. alexandrina* snails. We thank Shelley Cole and Vanessa Ayala (Texas Biomedical Research Institute) for help with MiSeq sequencing. This research was supported by a Forum grant (14-04491 (FC, WL), a Cowles fellowship (WL) from Texas Biomedical Research Institute and NIH grants (NIH R01AI133749 and R01AI123434 (TJCA)), and was conducted in facilities constructed with support from Research Facilities Improvement Program grant C06 RR013556 from the National Center for Research Resources.

CONFLICT OF INTEREST

The authors declare no conflict of interest.

REFERENCES

1. Lee W-J, Hase K. Gut microbiota-generated metabolites in animal health and disease. *Nature chemical biology* 2014; **10**: 416–424.
2. Kinross JM, Darzi AW, Nicholson JK. Gut microbiome-host interactions in health and disease. *Genome medicine* 2011; **3**: 14.
3. Oliver KM, Degnan PH, Burke GR, Moran NA. Facultative symbionts in aphids and the horizontal transfer of ecologically important traits. *Annual review of entomology* 2010; **55**: 247–266.
4. Hosokawa T, Koga R, Kikuchi Y, Meng X-Y, Fukatsu T. Wolbachia as a bacteriocyte-associated nutritional mutualist. *Proceedings of the National Academy of Sciences of the United States of America* 2010; **107**: 769–774.
5. Brune A. Symbiotic digestion of lignocellulose in termite guts. *Nature reviews Microbiology* 2014; **12**: 168–180.
6. Werren JH, Baldo L, Clark ME. Wolbachia: master manipulators of invertebrate biology. *Nature reviews Microbiology* 2008; **6**: 741–751.
7. Flintoft L. Evolution: Speciation meets microbiomes. *Nature reviews Genetics* 2013; **14**: 598.
8. Slatko BE, Luck AN, Dobson SL, Foster JM. *Wolbachia* endosymbionts and human disease control. *Molecular and biochemical parasitology* 2014; **195**: 88–95.
9. Sant'Anna MRV, Diaz-Albiter H, Aguiar-Martins K, Al Salem WS, Cavalcante RR, Dillon VM, et al. Colonisation resistance in the sand fly gut: *Leishmania* protects *Lutzomyia longipalpis* from bacterial infection. *Parasites & vectors* 2014; **7**: 329.
10. Stathopoulos S, Neafsey DE, Lawniczak MKN, Muskavitch MAT, Christophides GK. Genetic dissection of Anopheles gambiae gut epithelial responses to Serratia marcescens. *PLoS pathogens* 2014; **10**: e1003897.
11. WHO. World Health Organization. Schistosomiasis. https://www.who.int/news-room/fact-sheets/detail/schistosomiasis. Accessed 25 Mar 2020.

12. Colley DG, Bustinduy AL, Secor WE, King CH. Human schistosomiasis. *Lancet* 2014; **383**: 2253–2264.

13. van der Werf MJ, de Vlas SJ, Brooker S, Looman CWN, Nagelkerke NJD, Habbema JDF, et al. Quantification of clinical morbidity associated with schistosome infection in sub-Saharan Africa. *Acta Trop* 2003; **86**: 125–139.

14. Files VS, Cram EB. A study on the comparative susceptibility of snail vectors to strains of *Schistosoma mansoni*. *The Journal of Parasitology* 1949; **35**: 555–560.

15. Tennessen JA, Bonner KM, Bollmann SR, Johnstun JA, Yeh J-Y, Marine M, et al. Genome-Wide Scan and Test of Candidate Genes in the Snail Biomphalaria glabrata Reveal New Locus Influencing Resistance to Schistosoma mansoni. *PLoS Negl Trop Dis* 2015; **9**: e0004077.

16. Ducklow HW, Boyle PJ, Maugel PW, Strong C, Mitchell R. Bacterial flora of the schistosome vector snail *Biomphalaria glabrata*. *Appl Environ Microbiol* 1979; **38**: 667–672.

17. Allan ERO, Tennessen JA, Sharpton TJ, Blouin MS. Allelic variation in a single genomic region alters the microbiome of the snail *Biomphalaria glabrata*. *The Journal of heredity* 2018; **109**: 604–609.

18. Huot C, Clerissi C, Gourbal B, Galinier R, Duval D, Toulza E. Schistosomiasis vector snails and their microbiota display a phylosymbiosis pattern. *Frontiers in microbiology* 2019; **10**: 3092.

19. Desriac F, Le Chevalier P, Brillet B, Leguerinel I, Thuillier B, Paillard C, et al. Exploring the hologenome concept in marine bivalvia: haemolymph microbiota as a pertinent source of probiotics for aquaculture. *FEMS microbiology letters* 2014; **350**: 107–116.

20. Vezzulli L, Stagnaro L, Grande C, Tassistro G, Canesi L, Pruzzo C. Comparative 16SrDNA gene-based microbiota profiles of the pacific oyster (*Crassostrea gigas*) and the mediterranean mussel (*Mytilus galloprovincialis*) from a shellfish farm (ligurian sea, italy). *Microbial ecology* 2018; **75**: 495–504.

21. Lokmer A, Mathias Wegner K. Hemolymph microbiome of Pacific oysters in response to temperature, temperature stress and infection. *The ISME journal* 2015; **9**: 670–682.

22. Auguste M, Lasa A, Pallavicini A, Gualdi S, Vezzulli L, Canesi L. Exposure to TiO_2 nanoparticles induces shifts in the microbiota composition of *Mytilus galloprovincialis* hemolymph. *The Science of the total environment* 2019; **670**: 129–137.

23. Vezzulli L, Colwell RR, Pruzzo C. Ocean warming and spread of pathogenic vibrios in the aquatic environment. *Microbial ecology* 2013; **65**: 817–825.

24. Apprill A, McNally S, Parsons R, Weber L. Minor revision to V4 region SSU rRNA 806R gene primer greatly increases detection of SAR11 bacterioplankton. *Aquat Microb Ecol* 2015; **75**: 129–137.

25. Bolyen E, Rideout JR, Dillon MR, Bokulich NA, Abnet CC, Al-Ghalith GA, et al. Reproducible, interactive, scalable and extensible microbiome data science using QIIME 2. *Nature biotechnology* 2019; **37**: 852–857.

26. Fernandes AD, Reid JN, Macklaim JM, McMurrough TA, Edgell DR, Gloor GB. Unifying the analysis of high-throughput sequencing datasets: characterizing RNA-seq, 16S rRNA gene sequencing and selective growth experiments by compositional data analysis. *Microbiome* 2014; **2**: 15.

27. McMurdie PJ, Holmes S. phyloseq: an R package for reproducible interactive analysis and graphics of microbiome census data. *PloS one* 2013; **8**: e61217.

28. Kembel SW, Cowan PD, Helmus MR, Cornwell WK, Morlon H, Ackerly DD, et al. Picante: R tools for integrating phylogenies and ecology. *Bioinformatics (Oxford, England)* 2010; **26**: 1463–1464.

29. Větrovský T, Baldrian P. The variability of the 16S rRNA gene in bacterial genomes and its consequences for bacterial community analyses. *PloS one* 2013; **8**: e57923.

30. Valdes AM, Walter J, Segal E, Spector TD. Role of the gut microbiota in nutrition and health. *BMJ (Clinical research ed)* 2018; **361**: k2179.

31. Braquart-Varnier C, Lachat M, Herbinière J, Johnson M, Caubet Y, Bouchon D, et al. *Wolbachia* mediate variation of host immunocompetence. *PloS one* 2008; **3**: e3286.

32. Wang X-W, Wang J-X. Crustacean hemolymph microbiota: Endemic, tightly controlled, and utilization expectable. *Molecular immunology* 2015; **68**: 404–411.

33. Blow F, Douglas AE. The hemolymph microbiome of insects. *Journal of insect physiology* 2019; **115**: 33–39.

34. Swiatczak B, Cohen IR. Gut feelings of safety: tolerance to the microbiota mediated by innate immune receptors. *Microbiology and immunology* 2015; **59**: 573–585.

35. Bonner KM, Bayne CJ, Larson MK, Blouin MS. Effects of Cu/Zn superoxide dismutase (sod1) genotype and genetic background on growth, reproduction and defense in *Biomphalaria glabrata*. *PLoS NeglTrop Dis* 2012; **6**: e1701.

36. Ducklow HW, Clausen K, Mitchell R. Ecology of bacterial communities in the schistosomiasis vector snail *Biomphalaria glabrata*. *Microb Ecol* 1981; **7**: 253–274.

37. Jurberg P, Cunha RA, Rodrigues ML. Behavior of Biomphalaria glabrata Say, 1818 (Gastropoda: Planorbidae) - 1. Morphophysiology of the mantle cavity. *Memorias do Instituto Oswaldo Cruz* 1997; **92**: 287–295.

38. Sullivan JT, Cheng TC. Structure and function of the mantle cavity of Biomphalaria glabrata (Mollusca: Pulmonata). *Transactions of the American Microscopical Society* 1974; **93**: 416–420.

39. Sminia T, Barendsen L. A comparative morphological and enzyme histochemical study on blood cells of the freshwater snails Lymnaea stagnalis, Biomphalaria glabrata, and Bulinus truncatus. *Journal of morphology* 1980; **165**: 31–39.

40. Van Weel P. The comparative physiology of digestion in molluscs. *American Zoologist* 1961; 245–252.

41. Van Horn DJ, Garcia JR, Loker ES, Mitchell KR, Mkoji GM, Adema CM, et al. Complex intestinal bacterial communities in three species of planorbid snails. *Journal of Molluscan Studies* 2012; **78**: 74–80.

42. Richards CS. Two new species of Hartmannella amebae infecting freshwater mollusks. *The Journal of protozoology* 1968; **15**: 651–656.

43. Richards CS, Sheffield HG. Unique host relations and ultrastructure of a new microsporidian of the genus *Coccospora* infecting *Biomphalaria glabrata*. *Society for Invertebrate Pathology Newsletter* 1970; **2**: 12.

44. Stibbs HH, Owczarzak A, Bayne CJ, DeWan P. Schistosome sporocyst-killing amoebae isolated from *Biomphalaria glabrata*. *Journal of invertebrate pathology* 1979; **33**: 159–170.

45. Hertel LA, Bayne CJ, Loker ES. The symbiont *Capsaspora owczarzaki*, nov. gen. nov. sp., isolated from three strains of the pulmonate snail *Biomphalaria glabrata* is related to members of the Mesomycetozoea. *Int J Parasitol* 2002; **32**: 1183–1191.

46. Baron OL, van West P, Industri B, Ponchet M, Dubreuil G, Gourbal B, et al. Parental transfer of the antimicrobial protein LBP/BPI protects *Biomphalaria glabrata* eggs against oomycete infections. *PLoS pathogens* 2013; **9**: e1003792.

47. Hathaway JJM, Adema CM, Stout BA, Mobarak CD, Loker ES. Identification of protein components of egg masses indicates parental investment in immunoprotection of offspring by *Biomphalaria glabrata* (gastropoda, mollusca). *Dev Comp Immunol* 2010; **34**: 425–435.

48. Prado SS, Rubinoff D, Almeida RPP. Vertical transmission of a pentatomid caeca-associated symbiont. *Annals of the Entomological Society of America* 2006; **99**: 577–585.

49. Abe Y, Mishiro K, Takanashi M. Symbiont of brown-winged green bug, *Plautia stali* SCOTT. *Japanese journal of applied entomology and zoology* 1995; **39**: 109–115.

50. Stinson LF, Boyce MC, Payne MS, Keelan JA. The not-so-sterile womb: Evidence that the human fetus is exposed to bacteria prior to birth. *Frontiers in microbiology* 2019; **10**: 1124.

51. Vieira EC. Influence of vitamin E on reproduction of Biomphalaria glabrata under axenic conditions. *Am J Trop Med Hyg* 1967; **16**: 792–796.

52. Murray Stewart T, Dunston TT, Woster PM, Casero RA. Polyamine catabolism and oxidative damage. *The Journal of biological chemistry* 2018; **293**: 18736–18745.

53. Castillo MG, Humphries JE, Mourão MM, Marquez J, Gonzalez A, Montelongo CE. *Biomphalaria glabrata* immunity: Post-genome advances. *Developmental and comparative immunology* 2020; **104**: 103557.

54. Duval D, Galinier R, Mouahid G, Toulza E, Allienne JF, Portela J, et al. A novel bacterial pathogen of *Biomphalaria glabrata*: a potential weapon for schistosomiasis control? *PLoS neglected tropical diseases* 2015; **9**: e0003489.

55. Laidemitt MR, Zawadzki ET, Brant SV, Mutuku MW, Mkoji GM, Loker ES. Loads of trematodes: discovering hidden diversity of paramphistomoids in Kenyan ruminants. *Parasitology* 2017; **144**: 131–147.

56. Knight M, Miller A, Liu Y, Scaria P, Woodle M, Ittiprasert W. Polyethyleneimine (PEI) mediated siRNA gene silencing in the *Schistosoma mansoni* snail host, *Biomphalaria glabrata*. *PLoS neglected tropical diseases* 2011; **5**: e1212.

57. Allan ERO, Tennessen JA, Bollmann SR, Hanington PC, Bayne CJ, Blouin MS. Schistosome infectivity in the snail, *Biomphalaria glabrata*, is partially dependent on the expression of Grctm6, a Guadeloupe Resistance Complex protein. *PLoS neglected tropical diseases* 2017; **11**: e0005362.

58. Douglas AE. Simple animal models for microbiome research. *Nature reviews Microbiology* 2019; **17**: 764–775.

59. Paraense WL, Correa LR. Variation in susceptibility of populations of Australorbis glabratus to a strain of Schistosoma mansoni. *Rev Inst Med Trop Sao Paulo* 1963; **5**: 15–22.

60. Theron A, Rognon A, Gourbal B, Mitta G. Multi-parasite host susceptibility and multi-host parasite infectivity: A new approach of the *Biomphalaria glabrata/Schistosoma mansoni* compatibility polymorphism. *Infect Genet Evol* 2014; **26**: 80–88.

61. Lewis FA, Stirewalt MA, Souza CP, Gazzinelli G. Large-scale laboratory maintenance of *Schistosoma mansoni*, with observations on three schistosome/snail host combinations. *J Parasitol* 1986; **72**: 813–829.

FIGURES

Fig. 1 – Site of hemolymph sampling and workflow of the library preparation and the analysis. A. Snail hemolymph was sampled directly by heart puncture using a syringe. Left panel shows the position of the heart (arrow) on an albino snail. Right panel shows a schematic representation of the puncture. **B.** Work flow of the sample preparation and data processing.

Fig. 2 – Library rarefaction curve for each snail population. Curves represent the number of bacterial species identified while subsampling a defined number of 16S V4 sequences. Each curve reached a plateau phase indicating that sampling more sequences did not revealed new bacterial species and therefore that the sequencing was sufficient to capture all the diversity present in the hemolymph sample.

Fig. 3 – α diversity indices. Six different alpha diversity indices were computed (see Table 2 for index description) revealing that snail hemolymph harbors bacteria community and those community are richer and more diverse that those of the water. Variation in diversity exists between snail populations. All these bacterial communities are dominated by particular bacterial species.

Fig. 4 – Principal coordinates analysis (PCoA) of β diversity indices. For each index (A. Jaccard, B. Unweighted unifrac, C. Bray, D. Weighted unifrac), the first two axes of the PCoA are represented. The two first indices represent a qualitative measure (absence or presence of bacterial taxa) while the two last are quantitative (adjusted with taxa abundance). The matrices on the right side of each index showed the significance level of the Permanova test (differences between populations) and the β dispersion test (homogeneity of variance between populations). All four indices showed that water microbiome was different from snail hemolymph microbiomes, that the two species of snail (*B. glabrata* and *B. alexandrina*) can be differentiated on a quantitative and qualitative approaches, and that *B. glabrata* populations were differentiated based on rare taxa (qualitative

aspect) and this differentiation could be linked to their geographic origin. The ellipse represents the multivariate normal distribution.

Fig. 5 – Taxonomic diversity in each sample and populations. **A.** Dendrogram representing the distance between samples based on their microbiome composition. Number under each node represents bootstrap values from 1,000 iterations. Samples from the same population cluster together and links between populations reflects results obtained from the beta-diversity analysis. **B and C**. Relative abundance of the different phyla present in each samples from the dendrogram (B) and in each corresponding populations (C). Water microbiome showed dramatic differences when compared to snail hemolymph microbiomes. Snail microbiomes showed also specificities between populations.

Fig. 6 – Microbial density in each sample. **A.** Raw 16S copy number per microliter of hemolymph and water sample quantified using qPCR. **B.** Estimation of bacteria per microliter after adjusting 16S copy number using PiCRUST2 input. **C.** Correlation between observed number of ASVs and estimated bacteria number. The number of bacteria present in a sample does not correlate with the number of ASVs observed. The different letters indicate significant differences in density means (pairwise comparison post-hoc test, $p < 0.05$).

TABLES

Table 1 – Snail population used in this study and their characteristics.

***Biomphalaria* species**	***Biomphalaria* population**	**Origin (Country, town, snail cross)**	**Albinism**	**Inbreeding**	**References**
B. alexandrina	Ba	Egypt	No	No	Theodor Bilharz Research Institute, Egypt
B. glabrata	BgBS90	Brazil	No	No	[59]
	BgBRE	Brazil (Recife)	Yes	No	[60]
	BgNMRI	Puerto Rico	Yes	No	[61]
	Bg26	BgM line derived (cross between a Brazilian and a Puerto Rican snail)	Yes	Yes	[35]
	Bg36		Yes	Yes	
	Bg121		Yes	Yes	

Table 2 – Description of α diversity indices used.

Index	Description
Observed richness	Raw number of ASVs.
Chao1 richness	Estimation of the true richness by adjusting the raw number of ASVs for rare taxa.
Faith's Phylogenetic diversity index	Richness index adjusted with phylogenetic distance between ASVs.
Shannon index	Measure of heterogeneity in taxa representation (evenness × richness).
Simpson evenness index	Measure of true evenness of taxa within a sample independently of taxa richness. A value close to 0 means that the taxa are unevenly distributed in a sample.
Simpson dominance index	Measure of taxa diversity within a sample. This index is weighted towards the most abundant taxa and influenced by taxa richness. A value close to 0 means that the sample is dominated by few taxa.

SUPPLEMENTARY MATERIALS

Supp. Fig. 1 – Correlation of α diversity indices between replicates. For the six different alpha diversity indices, we performed a correlation analysis between the two replicates and showed that they are highly correlated confirming the reproducibility of our methods.

Supp. Fig. 2 – Heatmap of the 50 most abundant ASVs in each sample population. Some of the most abundant ASVs are unique to population.

Supp. Fig. 3 – Taxonomic diversity in each replicated samples. This figure is similar to Fig. 4 with the addition of the replicated libraries. Each replicated library clustered together showing the reproducibility of the protocol.

Supp. Table 1 – Earth Microbiome Project primers used for generating each library.

Supp. Table 2 – Library statistics.

Supp. Table 3 – Differentially represented metabolic pathways in snails and water samples.

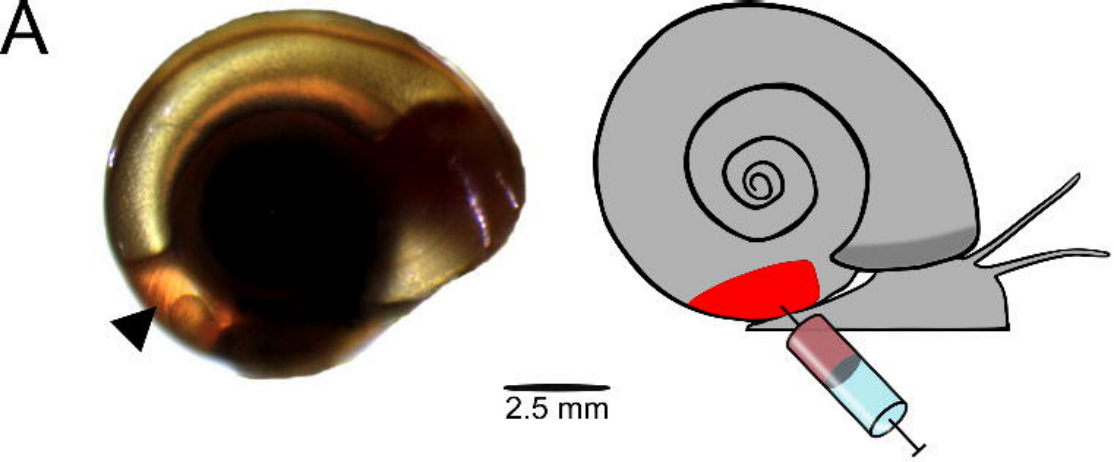
A
2.5 mm

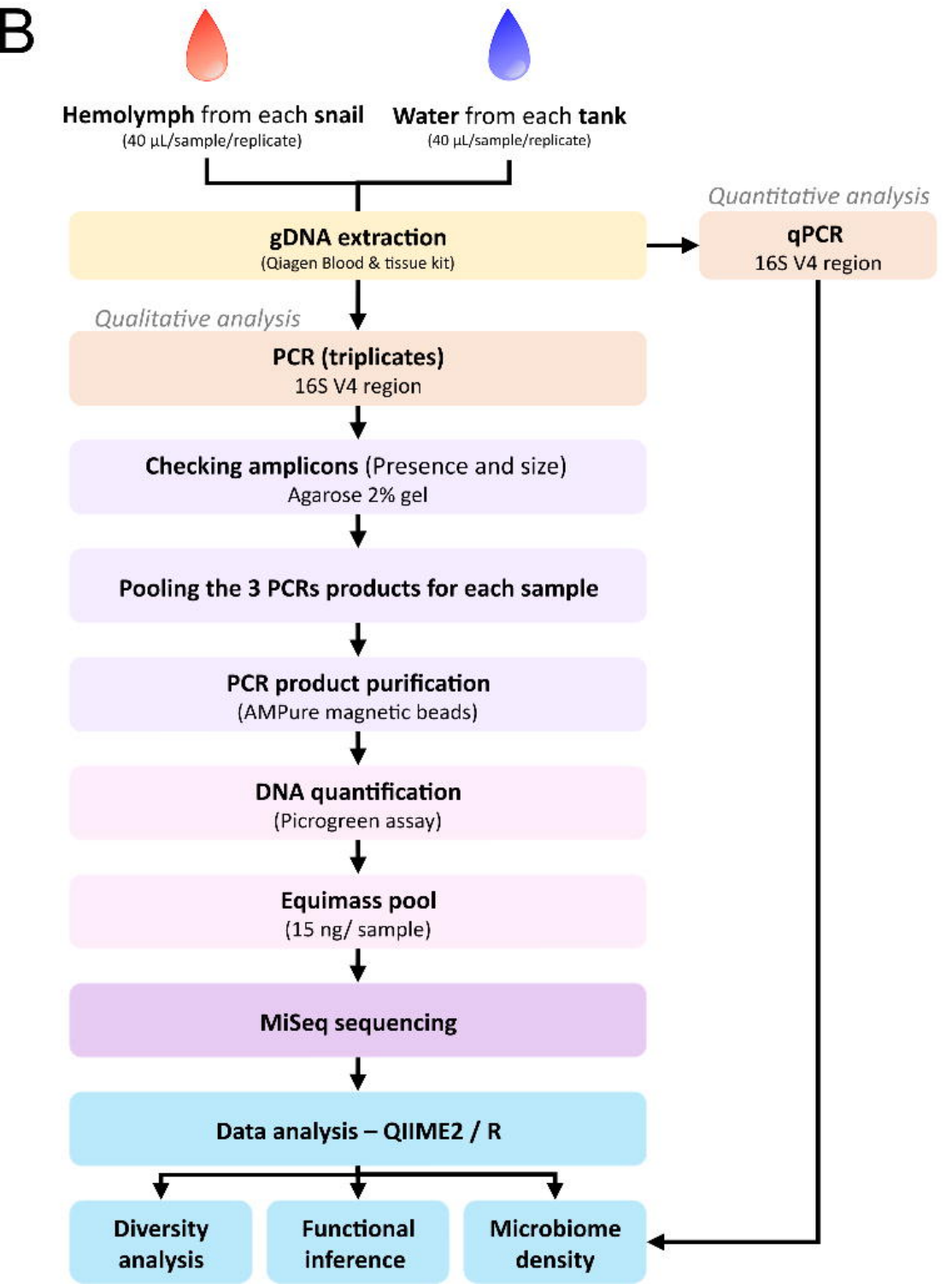
B
Hemolymph from each snail
(40 µL/sample/replicate)
Water from each tank
(40 µL/sample/replicate)
gDNA extraction
(Qiagen Blood & tissue kit)
Quantitative analysis
qPCR
16S V4 region
Qualitative analysis
PCR (triplicates)
16S V4 region
Checking amplicons (Presence and size)
Agarose 2% gel
Pooling the 3 PCRs products for each sample
PCR product purification
(AMPure magnetic beads)
DNA quantification
(Picrogreen assay)
Equimass pool
(15 ng/ sample)
MiSeq sequencing
Data analysis – QIIME2 / R
Diversity analysis
Functional inference
Microbiome density

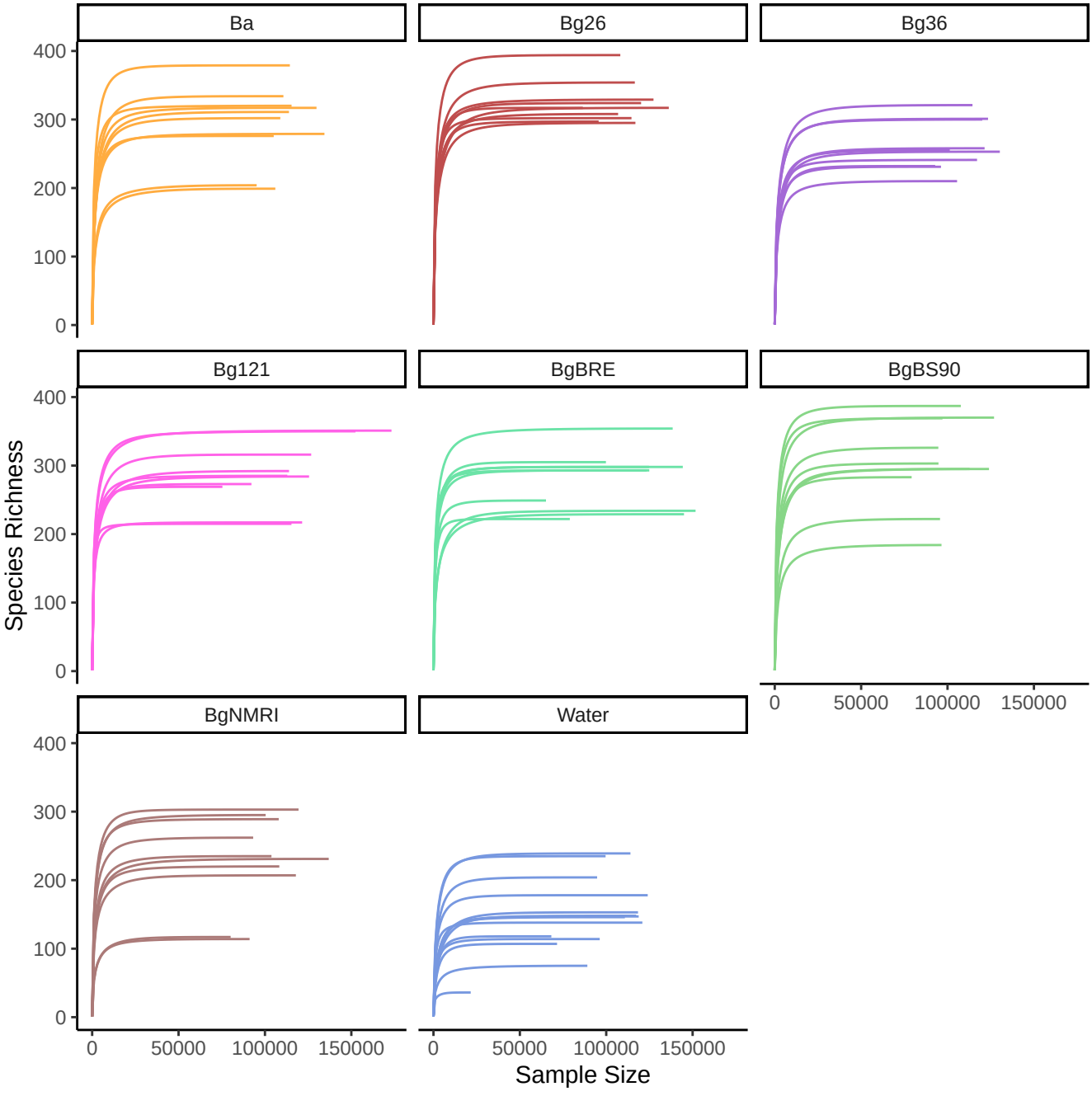
Ba
Bg26
Bg36
Bg121
BgBRE
BgBS90
BgNMRI
Water
Species Richness
Sample Size
0
100
200
300
400
0
50000
100000
150000

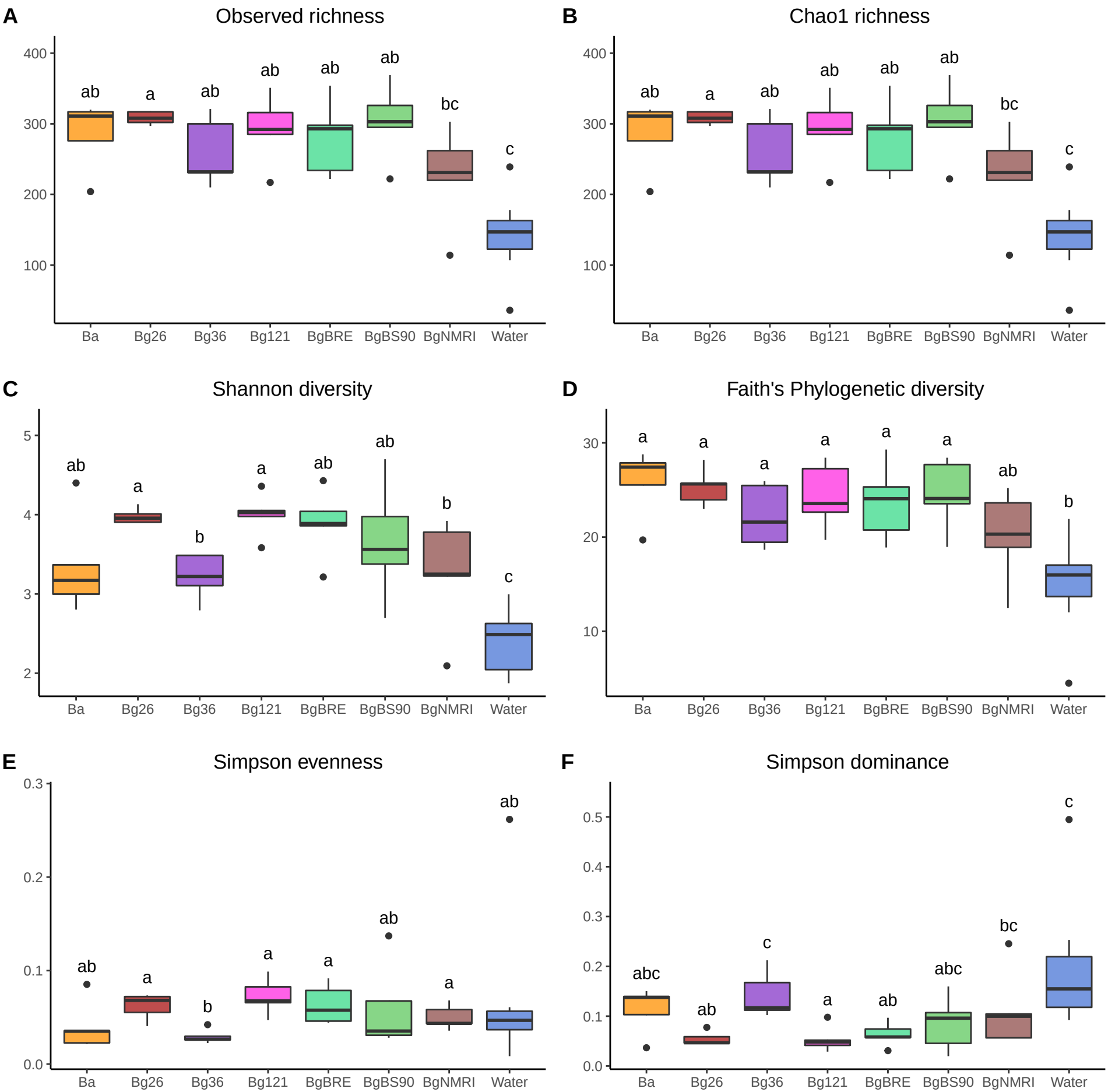
A
Observed richness
400
300
200
100
ab
a
ab
ab
ab
ab
bc
c
Ba
Bg26
Bg36
Bg121
BgBRE
BgBS90
BgNMRI
Water
B
Chao1 richness
400
300
200
100
ab
a
ab
ab
ab
ab
bc
c
Ba
Bg26
Bg36
Bg121
BgBRE
BgBS90
BgNMRI
Water
C
Shannon diversity
5
4
3
2
ab
a
b
a
ab
ab
b
c
Ba
Bg26
Bg36
Bg121
BgBRE
BgBS90
BgNMRI
Water
D
Faith's Phylogenetic diversity
30
20
10
a
a
a
a
a
a
ab
b
Ba
Bg26
Bg36
Bg121
BgBRE
BgBS90
BgNMRI
Water
E
Simpson evenness
0.3
0.2
0.1
0.0
ab
a
b
a
a
ab
a
ab
Ba
Bg26
Bg36
Bg121
BgBRE
BgBS90
BgNMRI
Water
F
Simpson dominance
0.5
0.4
0.3
0.2
0.1
0.0
abc
ab
c
a
ab
abc
bc
c
Ba
Bg26
Bg36
Bg121
BgBRE
BgBS90
BgNMRI
Water

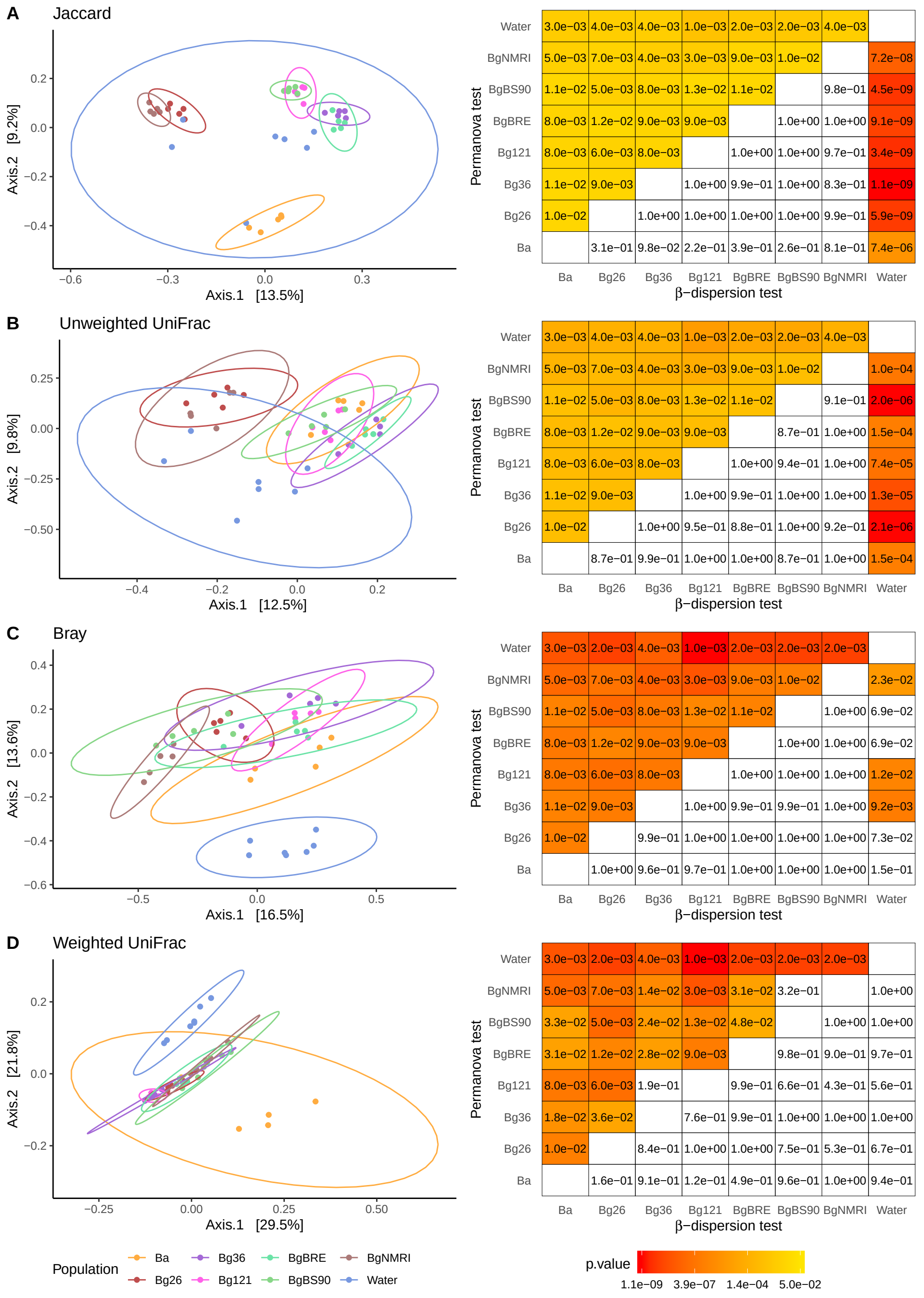
A
Jaccard
Axis.2 [9.2%]
Axis.1 [13.5%]
Permanova test
β−dispersion test
Water 3.0e−03 4.0e−03 4.0e−03 1.0e−03 2.0e−03 2.0e−03 4.0e−03
BgNMRI 5.0e−03 7.0e−03 4.0e−03 3.0e−03 9.0e−03 1.0e−02 7.2e−08
BgBS90 1.1e−02 5.0e−03 8.0e−03 1.3e−02 1.1e−02 9.8e−01 4.5e−09
BgBRE 8.0e−03 1.2e−02 9.0e−03 9.0e−03 1.0e+00 1.0e+00 9.1e−09
Bg121 8.0e−03 6.0e−03 8.0e−03 1.0e+00 1.0e+00 9.7e−01 3.4e−09
Bg36 1.1e−02 9.0e−03 1.0e+00 9.9e−01 1.0e+00 8.3e−01 1.1e−09
Bg26 1.0e−02 1.0e+00 1.0e+00 1.0e+00 1.0e+00 9.9e−01 5.9e−09
Ba 3.1e−01 9.8e−02 2.2e−01 3.9e−01 2.6e−01 8.1e−01 7.4e−06
Ba Bg26 Bg36 Bg121 BgBRE BgBS90 BgNMRI Water
B
Unweighted UniFrac
Axis.2 [9.8%]
Axis.1 [12.5%]
Permanova test
β−dispersion test
Water 3.0e−03 4.0e−03 4.0e−03 1.0e−03 2.0e−03 2.0e−03 4.0e−03
BgNMRI 5.0e−03 7.0e−03 4.0e−03 3.0e−03 9.0e−03 1.0e−02 1.0e−04
BgBS90 1.1e−02 5.0e−03 8.0e−03 1.3e−02 1.1e−02 9.1e−01 2.0e−06
BgBRE 8.0e−03 1.2e−02 9.0e−03 9.0e−03 8.7e−01 1.0e+00 1.5e−04
Bg121 8.0e−03 6.0e−03 8.0e−03 1.0e+00 9.4e−01 1.0e+00 7.4e−05
Bg36 1.1e−02 9.0e−03 1.0e+00 9.9e−01 1.0e+00 1.0e+00 1.3e−05
Bg26 1.0e−02 1.0e+00 9.5e−01 8.8e−01 1.0e+00 9.2e−01 2.1e−06
Ba 8.7e−01 9.9e−01 1.0e+00 1.0e+00 8.7e−01 1.0e+00 1.5e−04
Ba Bg26 Bg36 Bg121 BgBRE BgBS90 BgNMRI Water
C
Bray
Axis.2 [13.6%]
Axis.1 [16.5%]
Permanova test
β−dispersion test
Water 3.0e−03 2.0e−03 4.0e−03 1.0e−03 2.0e−03 2.0e−03 2.0e−03
BgNMRI 5.0e−03 7.0e−03 4.0e−03 3.0e−03 9.0e−03 1.0e−02 2.3e−02
BgBS90 1.1e−02 5.0e−03 8.0e−03 1.3e−02 1.1e−02 1.0e+00 6.9e−02
BgBRE 8.0e−03 1.2e−02 9.0e−03 9.0e−03 1.0e+00 1.0e+00 6.9e−02
Bg121 8.0e−03 6.0e−03 8.0e−03 1.0e+00 1.0e+00 1.0e+00 1.2e−02
Bg36 1.1e−02 9.0e−03 1.0e+00 9.9e−01 9.9e−01 1.0e+00 9.2e−03
Bg26 1.0e−02 9.9e−01 1.0e+00 1.0e+00 1.0e+00 1.0e+00 7.3e−02
Ba 1.0e+00 9.6e−01 9.7e−01 1.0e+00 1.0e+00 1.0e+00 1.5e−01
Ba Bg26 Bg36 Bg121 BgBRE BgBS90 BgNMRI Water
D
Weighted UniFrac
Axis.2 [21.8%]
Axis.1 [29.5%]
Permanova test
β−dispersion test
Water 3.0e−03 2.0e−03 4.0e−03 1.0e−03 2.0e−03 2.0e−03 2.0e−03
BgNMRI 5.0e−03 7.0e−03 1.4e−02 3.0e−03 3.1e−02 3.2e−01 1.0e+00
BgBS90 3.3e−02 5.0e−03 2.4e−02 1.3e−02 4.8e−02 1.0e+00 1.0e+00
BgBRE 3.1e−02 1.2e−02 2.8e−02 9.0e−03 9.8e−01 9.0e−01 9.7e−01
Bg121 8.0e−03 6.0e−03 1.9e−01 9.9e−01 6.6e−01 4.3e−01 5.6e−01
Bg36 1.8e−02 3.6e−02 7.6e−01 9.9e−01 1.0e+00 1.0e+00 1.0e+00
Bg26 1.0e−02 8.4e−01 1.0e+00 1.0e+00 7.5e−01 5.3e−01 6.7e−01
Ba 1.6e−01 9.1e−01 1.2e−01 4.9e−01 9.6e−01 1.0e+00 9.4e−01
Ba Bg26 Bg36 Bg121 BgBRE BgBS90 BgNMRI Water
Population
Ba Bg36 BgBRE BgNMRI
Bg26 Bg121 BgBS90 Water
p.value
1.1e−09 3.9e−07 1.4e−04 5.0e−02

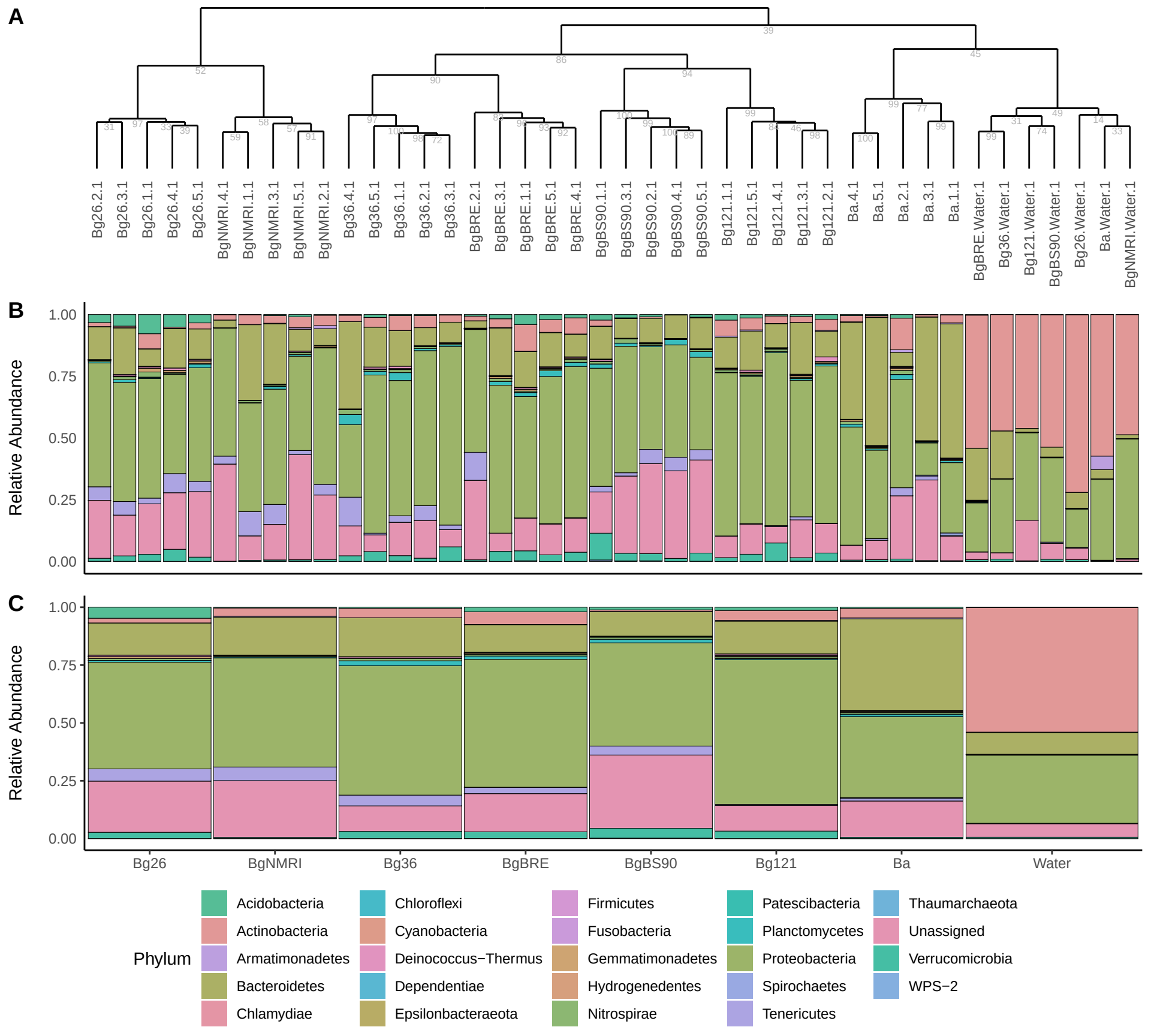
A
B
C
Relative Abundance
1.00
0.75
0.50
0.25
0.00
Bg26.2.1
Bg26.3.1
Bg26.1.1
Bg26.4.1
Bg26.5.1
BgNMRI.4.1
BgNMRI.1.1
BgNMRI.3.1
BgNMRI.5.1
BgNMRI.2.1
Bg36.4.1
Bg36.5.1
Bg36.1.1
Bg36.2.1
Bg36.3.1
BgBRE.2.1
BgBRE.3.1
BgBRE.1.1
BgBRE.5.1
BgBRE.4.1
BgBS90.1.1
BgBS90.3.1
BgBS90.2.1
BgBS90.4.1
BgBS90.5.1
Bg121.1.1
Bg121.5.1
Bg121.4.1
Bg121.3.1
Bg121.2.1
Ba.4.1
Ba.5.1
Ba.2.1
Ba.3.1
Ba.1.1
BgBRE.Water.1
Bg36.Water.1
Bg121.Water.1
BgBS90.Water.1
Bg26.Water.1
Ba.Water.1
BgNMRI.Water.1
Bg26
BgNMRI
Bg36
BgBRE
BgBS90
Bg121
Ba
Water
Phylum
Acidobacteria
Actinobacteria
Armatimonadetes
Bacteroidetes
Chlamydiae
Chloroflexi
Cyanobacteria
Deinococcus−Thermus
Dependentiae
Epsilonbacteraeota
Firmicutes
Fusobacteria
Gemmatimonadetes
Hydrogenedentes
Nitrospirae
Patescibacteria
Planctomycetes
Proteobacteria
Spirochaetes
Tenericutes
Thaumarchaeota
Unassigned
Verrucomicrobia
WPS−2

A
16S copy number per µL
10000
7500
5000
2500
0
ab
a
a
ab
b
ac
c
b
Ba
Bg26
Bg36
Bg121
BgBRE
BgBS90
BgNMRI
Water
B
Estimated number of bacteria per µL
10000
7500
5000
2500
0
ab
ab
ab
ab
a
ab
b
ab
Ba
Bg26
Bg36
Bg121
BgBRE
BgBS90
BgNMRI
Water
C
Number of observed ASVs
400
300
200
100
τ = −0.076 , p = 0.31
0
5000
10000
15000
Bacterial number